



## Research article

# Gold-selenide quantum dots supported onto cesium ferrite nanocomposites for the efficient degradation of rhodamine B

Fares T. Alshorifi <sup>a,b,\*</sup>, Abdullah A. Alswat <sup>c</sup>, Reda S. Salama <sup>d,\*\*</sup><sup>a</sup> Department of Chemistry, Faculty of Science, University of Saba Region, Yemen<sup>b</sup> Department of Chemistry, Faculty of Science, Sana'a University, Yemen<sup>c</sup> Chemistry Department, Faculty of Education and Applied Science, Arhab Sana'a University, Yemen<sup>d</sup> Basic Science Department, Faculty of Engineering, Delta University for Science and Technology, Gamasa, Egypt

## ARTICLE INFO

## Keywords:

AuSe quantum dots  
Quantum dots  
Water treatment  
Rhodamine B  
Ferrites

## ABSTRACT

In this work, different weight percentage of gold-selenide quantum dots (AuSe QDs) (1.0, 2.5, 5.0 and 7.0 wt.%) were successfully synthesized and decorated on cesium ferrite nanocomposite ( $\text{Cs}_2\text{Fe}_2\text{O}_4$  NC). The as-prepared pure AuSe QDs, pure  $\text{Cs}_2\text{Fe}_2\text{O}_4$  NC, and x wt.% AuSe QDs/ $\text{Cs}_2\text{Fe}_2\text{O}_4$  NC photocatalysts were investigated using different characterization techniques such as nitrogen adsorption desorption isotherms (BET), X-ray diffraction patterns (XRD), transmission electron microscopy (TEM), and UV-vis absorption spectroscopy. The results show that AuSe QDs were uniformly distributed on  $\text{Cs}_2\text{Fe}_2\text{O}_4$  NCs surface as spherical dots with an average size of 1.0–8.0 nm. While the  $\text{Cs}_2\text{Fe}_2\text{O}_4$  NCs possess an average size between 10 to 35 nm. The photocatalytic performance of x wt. % AuSe QDs/ $\text{Cs}_2\text{Fe}_2\text{O}_4$  NCs were measured through the photodegradation of rhodamine B (RhB) dye as a model water pollutant, under a 150 W-Mercury lamp with a filter (JB400) as a simulated source of visible light. The results revealed that the % degradation of RhB increased from 50.0 %, 59.1 %, 76.4 %, and to 99.15 % within 150 min for the pure  $\text{Cs}_2\text{Fe}_2\text{O}_4$ , 1.0, 2.5 and 5.0 wt.% AuSe QDs/ $\text{Cs}_2\text{Fe}_2\text{O}_4$  NC photocatalysts, respectively. The 5.0 wt.% AuSe/ $\text{Cs}_2\text{Fe}_2\text{O}_4$  NC sample showed highest photocatalytic activity. The effect of recycling also studied. High photocatalytic performance and superior stability confirmed that the prepared nanocomposites act as good photocatalysts.

## 1. Introduction

Nanotechnology is a rapidly growing field in which researchers deal with the synthesis and design of nanomaterials which are ranging from 1–100 nm [1, 2, 3, 4, 5]. The nanomaterials (NMs) have a remarkable differences in the catalytic, photocatalytic, biological and structural properties compared to the same materials in the bulk [6]. These differences in the nanomaterial's properties are due to differences in their size, shape and surface area with advancement in nanotechnology [7]. Quantum dots (QDs) [8, 9] have been attracted more attention of chemical researchers, may be due to their unique catalytic/photocatalytic capability in the chemical catalysis and the photocatalysis processes [10, 11, 12, 13]. The QDs have been extensively applied in the fields of environmental treatment/water treatment, chemical industry, sensors, solar cells, electronics, optoelectronics devices, cosmetics, drug delivery systems, and biological processes [10, 14, 15, 16, 17, 18]. There are many nanoparticles (NPs) such as CdSe, ZnSe,

CuSe, AgSe, Se, Ag, Cu, Au, Zn, and other metallic QDs which are coupled with/or supported on the magnetic composites [19, 20]. This coupling can be tuned to get the desired electrical, optical, and photocatalytic/catalytic properties on the surfaces of nanocomposites (NCs) [21, 22, 23, 24, 25, 26, 27, 28, 29, 30]. Thus, there is a need to develop green, rapid, and reliable experimental protocols for the synthesis of QDs, NCs or NPs [31, 32]. Precipitation method as a significant synthetic approach has many benefits over other methods. Thus, attention has been focused on the preparation of NMs using this approach [33].

Synthesis and coupling of metallic NPs with metallic ferrite materials [2, 39] are emerging as an alternative and efficient method for modifying their catalytic/photocatalytic, optical, and surface properties. Metallic ferrite materials have the following general formula  $M\text{Fe}_2\text{O}_4$ , where M sites are occupied by the bivalent cations such as  $\text{Mg}^{2+}$ ,  $\text{Co}^{2+}$ ,  $\text{Zn}^{2+}$ ,  $\text{Mn}^{2+}$ , and  $\text{Ca}^{2+}$  or by the monovalent cations such as  $\text{K}^{1+}$ ,  $\text{Cs}^{1+}$  and  $\text{Rb}^{1+}$ , while Fe ions are trivalent ( $\text{Fe}^{3+}$ ) [34, 35]. The metallic ferrite materials have remarkable electrical and magnetic properties as well as

\* Corresponding author.

\*\* Corresponding author.

E-mail addresses: [F.Alshareefi@su.edu.ye](mailto:F.Alshareefi@su.edu.ye), [amgdfareess@gmail.com](mailto:amgdfareess@gmail.com) (F.T. Alshorifi), [reda.salama@deltauniv.edu.eg](mailto:reda.salama@deltauniv.edu.eg), [dr.reda.salama@gmail.com](mailto:dr.reda.salama@gmail.com) (R.S. Salama).

their non-toxicity, cost-efficiency, and high stability, which can be used in numerous applications such as transformers, high-frequency devices, and quality filters. Recently, there are numerous techniques that are used for removing dyes from wastewater such as chemical oxidation [36, 37], biological treatment [38, 39], microwave catalysis [40, 41], adsorption [42, 43, 44, 45, 46, 47], and photochemical catalytic degradation [48, 49]. Each of these techniques has inherent advantages, and disadvantages. Photodegradation of the organic pollutants by various photocatalysts have reached good degradation efficiencies via tuning of catalyst structures, manipulation of particle sizes and introduction of metal dopants, but the photocatalysts still require further efforts toward high photocatalytic activity, selectivity, stability and durability for degradation of the chemical organic pollutants.

In this work, we attempt to open a new door in the photocatalytic degradation field by introducing synthesized AuSe QDs decorated  $\text{Cs}_2\text{Fe}_2\text{O}_4$  NC as novel photocatalysts for RhB degradation. The photocatalytic activity of catalysts is directly associated to the surface plasmon resonance phenomena (SPR), synergistic effect, and the band gap. By controlling the particle sizes, the electrons and holes are confined leading to an increase in the band gap, so this electron-holes confinement is referred to as quantum confinement. The QDs represent the same way as an individual atom. In fact, the band gap of nanoparticles increases as the particle sizes decrease. Thus, we tried to overcome this problem by immobilization AuSe QDs onto  $\text{Cs}_2\text{Fe}_2\text{O}_4$  NCs. Due to the synergistic effect, and the overlapping of Fermi level of AuSe QDs and magnetic  $\text{Cs}_2\text{Fe}_2\text{O}_4$  NCs, the separation of photogenerated holes and electrons will be significantly enhanced. Furthermore, several techniques have been used to investigate the chemical, optical and surface plasmon resonance and photocatalytic properties of the prepared photocatalysts using XRD, TEM, UV-visible spectroscopy, and BET.

## 2. Experimental

### 2.1. Materials

Sodium borohydride ( $\text{NaBH}_4$ , >98%), iron (III) nitrate ( $\text{Fe}(\text{NO}_3)_3 \cdot 9\text{H}_2\text{O}$ , >99%), and cesium nitrate ( $\text{CsNO}_3$ , >99%) were obtained from Sigma Aldrich, while Selenium chloride and Gold (III) chloride hydrate were obtained from Merck.

### 2.2. Synthesis of $\text{Cs}_2\text{Fe}_2\text{O}_4$ composite

Firstly, 10 mmol of  $\text{CsNO}_3$  and 20 mmol of  $\text{Fe}(\text{NO}_3)_3 \cdot 9\text{H}_2\text{O}$  were added to 50 ml of distilled water under vigorously stirring followed by addition of 50 ml of 2.0 M NaOH solution under constant stirring for 30 min. In the next step, the resultant mixture was concentrated on a water bath at 80 °C with continuous stirring until the formation of brown gel. Then, the brown gel was washed three times, centrifuged and dried at 110 °C overnight. Finally, the resultant brown powder was calcined at 400 °C for 4 h [10, 35, 50].

### 2.3. Fabrication of x wt.% AuSe QDs/ $\text{Cs}_2\text{Fe}_2\text{O}_4$ NCs

Firstly, AuSe QDs were prepared as previously reported literature with some modification [51]. 5.0 mmol of gold chloride and 5.0 mmol of selenium chloride were dissolved in distilled-H<sub>2</sub>O (40 mL) and transferred into 250 mL round bottom flask. Then  $\text{NaBH}_4$  solution was added dropwise to the above solution with constant stirring for 30 min. Finally, the formed precipitate was collected by centrifugation at 4000 rpm and washed with anhydrous ethanol and distilled water, then dried at 80 °C.

To fabrication of x wt.% AuSe QDs/ $\text{Cs}_2\text{Fe}_2\text{O}_4$  NCs, an appropriate amount of AuSe QDs (previously prepared) were dispersed in solution (50 mL) containing 10 mmol of  $\text{CsNO}_3$  and 20 mmol of  $\text{Fe}(\text{NO}_3)_3 \cdot 9\text{H}_2\text{O}$  and sonicated for 30 min. After that, 50 mL of 2.0 M NaOH were added to the previous solution under vigorous stirring, then the resultant hydrogel was moved into an autoclave and heated at 150 °C for 4 h. The formed

precipitate was centrifuged at 4000 rpm and washed with distilled water, then dried in an oven at 80 °C. The x wt.% AuSe QDs/ $\text{Cs}_2\text{Fe}_2\text{O}_4$  NCs with various weight percentage of AuSe QDs (1.0, 2.5, 5.0 and 7.0 wt. %) were prepared and marked as 1-ACFO, 2.5-ACFO, 5-ACFO, and 7-ACFO, respectively.

### 2.4. Characterization techniques

The crystal composition and chemical structure of pure AuSe QDs and AuSe QDs/ $\text{Cs}_2\text{Fe}_2\text{O}_4$  NCs were confirmed by XRD patterns using PW150 (Philips) with Cu (K $\alpha$ )-XR-radiation source ( $\lambda = 0.1541$  nm) at 45 mA and 40 KV. The particle morphology and size of the AuSe QDs/ $\text{Cs}_2\text{Fe}_2\text{O}_4$  NCs, were investigated through TEM-(Jeol-Jem-2100). Nitrogen adsorption/desorption isotherms were used to measure the specific surface area of these prepared composites which was determined at 77 K on a volumetric instrument (Micromeritics ASAP 2020, USA). The optical properties of the as-synthesized photocatalysts were measured using UV-Visible spectrometry.

### 2.5. Photocatalytic degradation process

The photocatalytic experiments carried out under a 150 W-mercury lamp with a filter (JB400) as a simulated visible-light source. The reaction mixture contained 0.1 g of the prepared photocatalysts in 40 mL RhB (10 ppm) and was placed in a quartz pipe in the middle of the reactor and irradiated by a Hg Lamp (150 W). The reaction performed in dark for 30 min to determine the adsorption rate on surface of AuSe QDs/ $\text{Cs}_2\text{Fe}_2\text{O}_4$  NC photocatalysts, after that it irradiated for a definite time until the complete degradation of the RhB. Finally, the remained dye concentration measured using UV-Visible spectrometry.

## 3. Result and discussion

### 3.1. XRD analysis

The crystalline phases of AuSe QDs,  $\text{Cs}_2\text{Fe}_2\text{O}_4$  and 5.0 wt. % AuSe QDs/ $\text{Cs}_2\text{Fe}_2\text{O}_4$  NC were analyzed by XRD spectrum. Figure 1 (a) shows that the diffraction peaks at  $2\theta$  equal 38° (111), 42° (200), 64° (220), and 78° (311) were observed for the AuSe QDs in accordance with Beta-structure  $\beta$ -AuSe (JCPDS card 00-020-0458) [32, 52] and very small two peaks of the  $\alpha$ -AuSe as well appeared. This confirms the formation of crystalline  $\beta$ -AuSe QDs. No other peaks that ascribed to any impurity are detected. Also, XRD patterns for pure  $\text{Cs}_2\text{Fe}_2\text{O}_4$  and 5.0 wt.% AuSe QDs/ $\text{Cs}_2\text{Fe}_2\text{O}_4$  NCs were displayed in Figure 1 (b and c). The patterns of Bragg reflection of the  $\text{Cs}_2\text{Fe}_2\text{O}_4$  NC observed at  $2\theta$  angle equal 18.30,

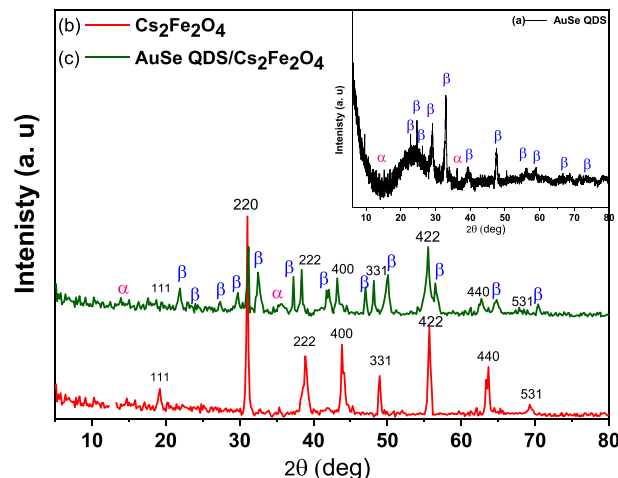


Figure 1. XRD patterns of (a) Pure AuSe QDs, (b) Pure  $\text{Cs}_2\text{Fe}_2\text{O}_4$  NC and (c) 5.0 wt. % AuSe QDs/ $\text{Cs}_2\text{Fe}_2\text{O}_4$  NC.

38.26, 43.36, 48.21, 54.95, 63.06 and 68.4° [34, 53]. The patterns suggested that the  $\text{Cs}_2\text{Fe}_2\text{O}_4$  peaks have a crystalline nature referring to different reflections of the cubic  $\text{Cs}_2\text{Fe}_2\text{O}_4$  phase. No other peaks that ascribed to any impurity are detected. Further, the successful synthesis of pure  $\text{Cs}_2\text{Fe}_2\text{O}_4$  NC was verified. These peaks are well agreed with previously reported literature [34, 53]. On the other hand, the peak patterns of 5.0 wt. % AuSe QDs/ $\text{Cs}_2\text{Fe}_2\text{O}_4$  NC were similar to the pure  $\text{Cs}_2\text{Fe}_2\text{O}_4$  peaks, and in addition to that some new peaks were appeared. The peaks obtained in the pattern are matched with the standard  $\beta$ -AuSe QDs [32, 52], and the standard  $\text{Cs}_2\text{Fe}_2\text{O}_4$  NC, indicating to coexistence of  $\beta$ -AuSe QDs and  $\text{Cs}_2\text{Fe}_2\text{O}_4$  NC as AuSe QDs/ $\text{Cs}_2\text{Fe}_2\text{O}_4$  NC. The changing of the relative peak intensity of the  $\text{Cs}_2\text{Fe}_2\text{O}_4$  NC indicated that the addition of AuSe QDs inhibits the crystal growth of the  $\text{Cs}_2\text{Fe}_2\text{O}_4$  nanoparticles that produce smaller crystalline sizes compared to unmodified  $\text{Cs}_2\text{Fe}_2\text{O}_4$  NC. Furthermore, there is no diffraction peak except the diffraction peaks attributed to  $\text{Cs}_2\text{Fe}_2\text{O}_4$  NC and  $\beta$ -AuSe QDs, which indicated that the as-synthesized AuSe QDs/ $\text{Cs}_2\text{Fe}_2\text{O}_4$  NC was not including any impurities. The average crystallite sizes of the as-synthesized AuSe QDs,  $\text{Cs}_2\text{Fe}_2\text{O}_4$ , and 5.0 wt. % AuSe QDs/ $\text{Cs}_2\text{Fe}_2\text{O}_4$  NC was calculated by Scherer equation and found between 1-8 nm of AuSe QDs and between 10-35 nm of Nano-sized  $\text{Cs}_2\text{Fe}_2\text{O}_4$  composite.

### 3.2. Transmission electron microscopy (TEM)

The TEM images of the pure AuSe QDs and 5.0 wt. % AuSe QDs/ $\text{Cs}_2\text{Fe}_2\text{O}_4$  NC were shown in Figure 2. The TEM images displayed that pure AuSe QDs appeared as dots on the surface of  $\text{Cs}_2\text{Fe}_2\text{O}_4$  NC, which confirmed the existence of AuSe QDs on  $\text{Cs}_2\text{Fe}_2\text{O}_4$  surface. The sizes of spherical  $\text{Cs}_2\text{Fe}_2\text{O}_4$  nanoparticles were ranged between 10.32- 35.08 nm, while the sizes of AuSe QDs were 1.18-8.69 nm. Also, the TEM images displayed that there is no clear accumulation of AuSe QDs on the surface of  $\text{Cs}_2\text{Fe}_2\text{O}_4$  NC, as well as the AuSe QDs were well suspended in deionized water and were facile to disperse on the  $\text{Cs}_2\text{Fe}_2\text{O}_4$  surface. The  $\text{Cs}_2\text{Fe}_2\text{O}_4$  NC played a more important role in the dispersion process of the AuSe QDs on its surface due to their magnetic properties. The results confirm that the spherical  $\text{Cs}_2\text{Fe}_2\text{O}_4$  structure did not changed even after loading AuSe QDs on its surface as it displayed in XRD analysis. Based on the size distribution histograms of particles as shown in Figure 3, the average sizes of AuSe QDs were found to be 3.6 nm, while the average sizes of  $\text{Cs}_2\text{Fe}_2\text{O}_4$  NC were equal 25.4 nm.

### 3.3. UV-visible spectroscopy

The energy band structure and optical absorption properties of the prepared AuSe QDs/ $\text{Cs}_2\text{Fe}_2\text{O}_4$  NCs were investigated by UV/Vis diffuse reflectance spectra as shown in Figure 4. The figure revealed that there was a good absorption ability for visible light by both pure AuSe QDs and pure  $\text{Cs}_2\text{Fe}_2\text{O}_4$  NC. Also, the absorbance curves of pure AuSe QDs and AuSe QDs/ $\text{Cs}_2\text{Fe}_2\text{O}_4$  NCs have absorption curves reached to 743 nm. The prepared AuSe QDs/ $\text{Cs}_2\text{Fe}_2\text{O}_4$  photocatalysts showed better optical absorption than pure AuSe QDs and pure  $\text{Cs}_2\text{Fe}_2\text{O}_4$  NC, which in its turn improved the efficiency toward visible light. Figure 4 showed an obvious shifting with a wavelength from 462 nm to 565 nm in AuSe QDs/ $\text{Cs}_2\text{Fe}_2\text{O}_4$  NC. These results revealed that the visible light absorption properties of the  $\text{Cs}_2\text{Fe}_2\text{O}_4$  NC improved after loading of different AuSe QDs percentages. The enhanced absorption of x wt. % AuSe QDs/ $\text{Cs}_2\text{Fe}_2\text{O}_4$  NCs can be attributed to the surface Plasmon resonance effect of AuSe QDs originating from the interaction of the magnetic and electric field of light on the surface of AuSe QDs/ $\text{Cs}_2\text{Fe}_2\text{O}_4$  NCs. This SPR and synergistic effect of AuSe QDs and  $\text{Cs}_2\text{Fe}_2\text{O}_4$  can be used to sensitize these photocatalysts to enhance the optical and photocatalytic properties, so it will enhance the visible light-photocatalytic performance of x wt.% AuSe QDs/ $\text{Cs}_2\text{Fe}_2\text{O}_4$  NCs. The SPR band recommended that the prepared AuSe QDs supported on the  $\text{Cs}_2\text{Fe}_2\text{O}_4$  surface were almost small dots shape, which were confirmed by XRD and TEM images. The addition of AuSe QDs on the  $\text{Cs}_2\text{Fe}_2\text{O}_4$  led to increasing in the absorption intensity in the

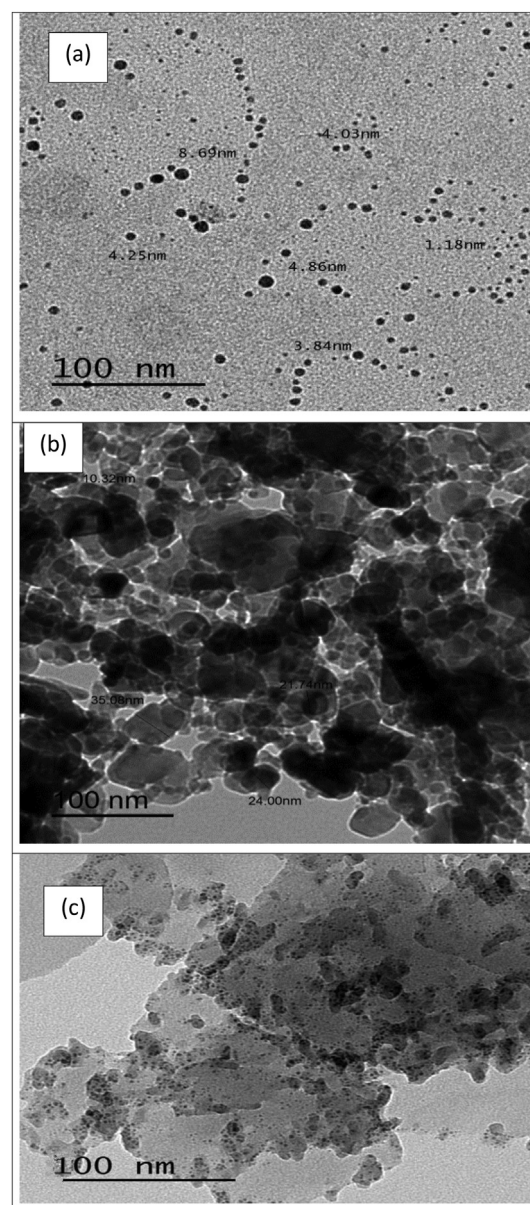


**Figure 2.** TEM images of (a) pure AuSe QDs, (b) pure  $\text{Cs}_2\text{Fe}_2\text{O}_4$  NC and (c) 5.0 wt.% AuSe QDs/ $\text{Cs}_2\text{Fe}_2\text{O}_4$  NC.

SPR band with shifted into a higher wavelength. From Figure 4, we can also observe that 5.0 wt. % AuSe QDs/ $\text{Cs}_2\text{Fe}_2\text{O}_4$  NC reflected the strongest-SPR at a broad absorption peak centering at 545 nm, which was considered the largest absorption in the visible region (it's broad from 400 nm to 740 nm). And one of the most important factors that affected on SPR band was particle size. Because of AuSe QDs have a smaller size, it is not hard to understand that the x % AuSe QDs/ $\text{Cs}_2\text{Fe}_2\text{O}_4$  NCs displayed the largest visible absorption and the strongest SPR, compared with the pure  $\text{Cs}_2\text{Fe}_2\text{O}_4$  NC.

Furthermore, the band gap energy of AuSe QDs/ $\text{Cs}_2\text{Fe}_2\text{O}_4$  NC samples were calculated according to the Kubelka-Munc equation [ $\alpha h\nu = A(h\nu - Eg)^{n/2}$ ]. Figure 5 displayed that were two regions demonstrating the two optical absorption edges ( $E_g1$  and  $E_g2$ ), double energy gap, for AuSe QDs/ $\text{Cs}_2\text{Fe}_2\text{O}_4$  NCs as described by many authors [54, 55, 56]. The presence of two energy gaps ascribed to the optical transitions from the valence sub-bands to the conduction band minimum, i.e., overlapping of Fermi levels of both AuSe QDs and  $\text{Cs}_2\text{Fe}_2\text{O}_4$  nanoparticles. The band gap values showed decrease with increasing of AuSe QDs content on the  $\text{Cs}_2\text{Fe}_2\text{O}_4$  surface as are seen in Fig .5. The energy gap of pure AuSe QDs, pure

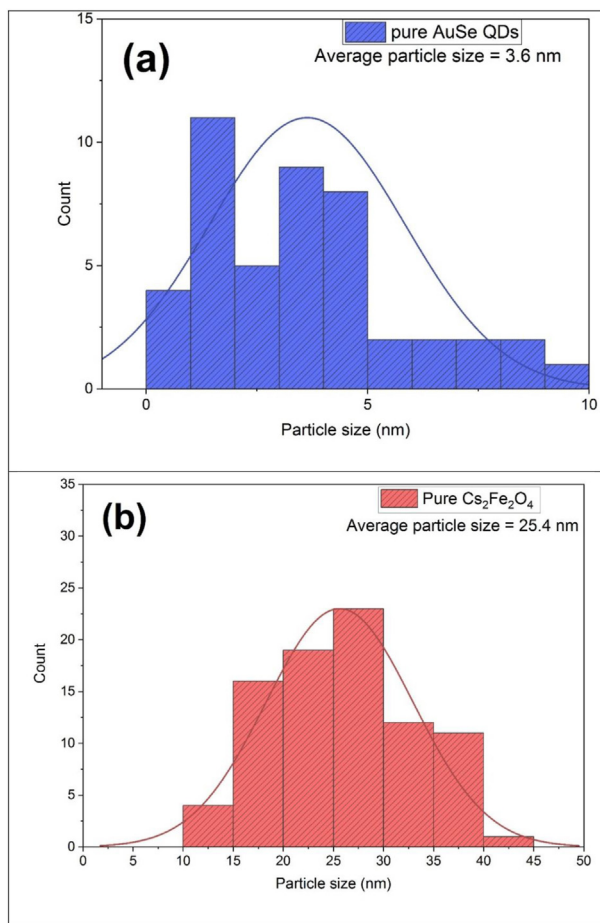


**Figure 3.** Nanoparticle size distribution histograms for (a) pure AuSe QDs, (b) pure  $\text{Cs}_2\text{Fe}_2\text{O}_4$  NC and (c) 5.0 wt.% AuSe QDs/ $\text{Cs}_2\text{Fe}_2\text{O}_4$  NC.

$\text{Cs}_2\text{Fe}_2\text{O}_4$ , 1-ACFO, 2.5-ACFO and 5-ACFO was measured and showed in Table 1. It was observed that the values of energy band gap  $E_{g2}$  in case of direct and indirect allowed transition decrease with increasing of AuSe QDs. However, values of energy band gap  $E_{g1}$  in case of both transitions are close to each other and slightly changed with AuSe QDs contents. It was found that  $E_{g1}$  of AuSe QDs/ $\text{Cs}_2\text{Fe}_2\text{O}_4$  NCs ranged from 1.79 eV to 2.06 eV compared with  $E_{g1}$  of the pure  $\text{Cs}_2\text{Fe}_2\text{O}_4$  NC (3.2 eV) and pure AuSe QDs (2.13 eV). And the presence of a new band provided

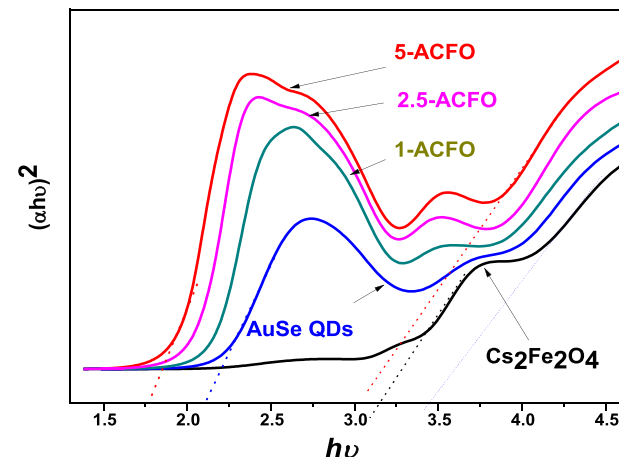


**Figure 5.**  $(\alpha h\nu)^{1/2}$  versus photon energy ( $h\nu$ ) for pure AuSe QDs, pure  $\text{Cs}_2\text{Fe}_2\text{O}_4$  and x wt.% AuSe QDs/ $\text{Cs}_2\text{Fe}_2\text{O}_4$  NCs.

strong evidence that AuSe QDs have successfully embedded on the  $\text{Cs}_2\text{Fe}_2\text{O}_4$  NC.

### 3.4. Textural measurement (BET)

Nitrogen adsorption desorption isotherms of the as-synthesized  $\text{Cs}_2\text{Fe}_2\text{O}_4$  NC and x wt.% AuSe QDs/ $\text{Cs}_2\text{Fe}_2\text{O}_4$  NC samples were displayed in Figure 6, which exhibited type-IV isotherms according to IUPAC classification [57, 58, 59] and have inflection around  $P/P^0$  (0.20–0.40) with narrow hysteresis loops. The specific surface area of the  $\text{Cs}_2\text{Fe}_2\text{O}_4$  NC and x wt.% AuSe QDs/ $\text{Cs}_2\text{Fe}_2\text{O}_4$  NCs was calculated from the isotherms. The x wt.% AuSe QDs/ $\text{Cs}_2\text{Fe}_2\text{O}_4$  NC samples exhibited a slightly smaller BET surface area than that of pure  $\text{Cs}_2\text{Fe}_2\text{O}_4$  NC (18.70  $\text{m}^2/\text{g}$ ). For the sample of 1.0, 2.5, and 5.0 wt. % AuSe QDs/ $\text{Cs}_2\text{Fe}_2\text{O}_4$  NC, the BET surface area was equal to 15.43, 13.51 and 11.27  $\text{m}^2/\text{g}$ , respectively. These results are in the same order of magnitude, inducting that loading of x wt.% AuSe QDs on the  $\text{Cs}_2\text{Fe}_2\text{O}_4$  surface affected on the surface area. Meanwhile, there is a correlation between the AuSe QDs content and the surface area value, which was observed. It is clear from Figure 6, the adsorption capacity of x wt.% AuSe QDs/ $\text{Cs}_2\text{Fe}_2\text{O}_4$  NCs was decreased with increasing of the AuSe QDs content, which could be related to the deposition of AuSe QDs on both the surface and pores of  $\text{Cs}_2\text{Fe}_2\text{O}_4$  NC [60, 61, 62].

### 3.5. Photocatalytic activity

The photocatalytic performance of the prepared AuSe QDs/ $\text{Cs}_2\text{Fe}_2\text{O}_4$  NC catalysts was estimated by monitoring the photodegradation of organic RhB dyes under simulated visible light irradiation in an aqueous solution. The degradation of RhB versus reaction time displayed in Figure 7. The degradation ratios were gradually decreased with increasing of the reacting time, which indicated that the RhB has been significantly decomposed by x wt.% AuSe QDs/ $\text{Cs}_2\text{Fe}_2\text{O}_4$  photocatalysts. The photocatalytic activity of the pure  $\text{Cs}_2\text{Fe}_2\text{O}_4$ , 1.0, 2.5, 5.0 wt.% AuSe QDs/ $\text{Cs}_2\text{Fe}_2\text{O}_4$  NC samples for degradation of RhB dye was 50.0 %, 59.1 %, 76.4 %, and 99.15 % after 150 min under visible light, respectively. Enhancement of the degradation ratio indicated that the heterostructure AuSe QDs/ $\text{Cs}_2\text{Fe}_2\text{O}_4$  NC efficiently increased, which induced the

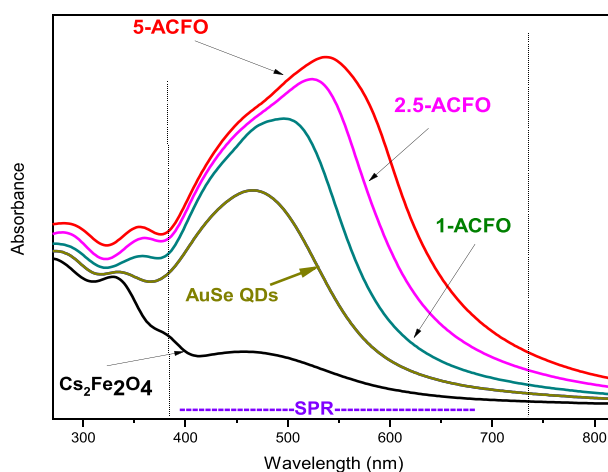


**Figure 4.** UV-vis. absorption spectra of pure AuSe QDs, pure  $\text{Cs}_2\text{Fe}_2\text{O}_4$  and x wt.% AuSe QDs/ $\text{Cs}_2\text{Fe}_2\text{O}_4$  NCs.

**Table 1.**  $E_{g1}$  and  $E_{g2}$  (energy gap) of the prepared samples.

	AuSe QDs	$\text{Cs}_2\text{Fe}_2\text{O}_4$	1-ACFO	2.5-ACFO	5-ACFO
$E_{g1}$	2.66	3.49	3.30	3.17	3.04
$E_{g2}$	2.13	3.21	2.06	1.96	1.79

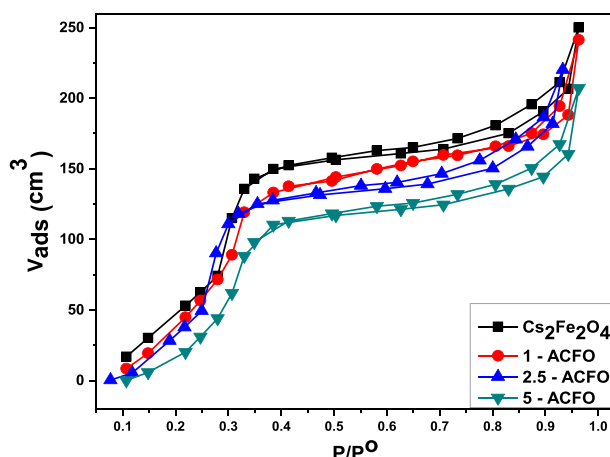


**Figure 6.** Nitrogen adsorption/desorption isotherms of pure  $\text{Cs}_2\text{Fe}_2\text{O}_4$  NC and  $x$  wt.% AuSe QDs/ $\text{Cs}_2\text{Fe}_2\text{O}_4$  NCs.

separation of photogenerated holes and electrons after the addition of AuSe QDs on the  $\text{Cs}_2\text{Fe}_2\text{O}_4$  surface.

The results indicated that the AuSe QDs content played a significant role in the enhancement of photocatalytic properties of AuSe QDs/ $\text{Cs}_2\text{Fe}_2\text{O}_4$  photocatalysts, due to the AuSe QDs having the ability to trap electrons, so the real separation of electron-hole pairs occurred. This confirmed that there was overlapping between Fermi levels of both the AuSe QDs and  $\text{Cs}_2\text{Fe}_2\text{O}_4$  NC which in turn led to decrease in the band gap with increasing the AuSe QDs content. On the other hand, the decrease in the pore diameter with increasing the AuSe QDs content led to promote photocatalytic activity due to the AuSe QDs diffuse through the entire pores and surface of AuSe QDs/ $\text{Cs}_2\text{Fe}_2\text{O}_4$  photocatalyst, so, there will be more available active sites on the AuSe QDs/ $\text{Cs}_2\text{Fe}_2\text{O}_4$  surface. This meant that the higher photocatalytic activity may be attributed to increasing the available active sites on the AuSe QDs/ $\text{Cs}_2\text{Fe}_2\text{O}_4$  surface. The photocatalytic degradation of RhB dye by 5.0 wt. % AuSe QDs/ $\text{Cs}_2\text{Fe}_2\text{O}_4$  NC sample was the highest. The existence of AuSe QDs on the  $\text{Cs}_2\text{Fe}_2\text{O}_4$  NC made the excited electron easily transferred into the surface of AuSe QDs/ $\text{Cs}_2\text{Fe}_2\text{O}_4$  catalyst. These surface electrons can be reacted with the oxygen molecules to produce  $\text{O}_2^\bullet$  radicals, while the positive charges (the holes) can be reacted with the water molecules to produce

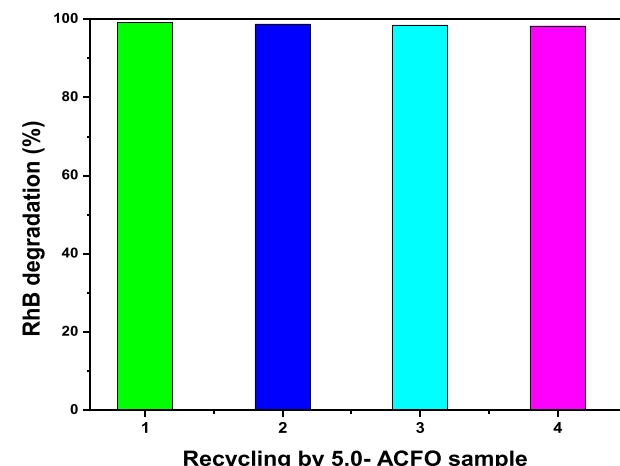


**Figure 8.** Reusability test over 5.0 wt.% AuSe QDs/ $\text{Cs}_2\text{Fe}_2\text{O}_4$  NC.

the  $\text{OH}^\bullet$  radicals. These radicals led to the degradation of RhB dye easily. The stability of the as-synthesized 5.0 wt.% AuSe QDs/ $\text{Cs}_2\text{Fe}_2\text{O}_4$  NC was testified for four cycles under the same condition and using 0.1 g of the photocatalyst. The results revealed that the photodegradation of RhB dye reached to 98.25 % after four cycles as shown in Figure 8. This decrease could be due to the decreasing surface interaction between the reaction intermediates in the photodegradation process of RhB dye. This results obviously revealed the excellent stability of 5.0 wt. % AuSe QDs/ $\text{Cs}_2\text{Fe}_2\text{O}_4$  NC as an excellent heterogenous photocatalyst as well. We can conclude by stating that the fabrication and high photocatalytic performance of  $x$  wt.% AuSe QDs/ $\text{Cs}_2\text{Fe}_2\text{O}_4$  NC photocatalysts have been realized in this work.

#### 4. Conclusion

This study described a green and efficient pathway for gold selenide quantum dots and cesium ferrite nanocomposite. In summary, novel AuSe QDs/ $\text{Cs}_2\text{Fe}_2\text{O}_4$  NCs with the visible light response were successfully prepared. The heterogeneous  $x$  wt. % AuSe QDs/ $\text{Cs}_2\text{Fe}_2\text{O}_4$  NCs were applied for photocatalytic degradation of RhB dye in the aqueous solution. The results displayed that the photocatalytic activity of AuSe QDs/ $\text{Cs}_2\text{Fe}_2\text{O}_4$  NCs was improved after loading different mass ratios of AuSe QDs content (1.0, 3.0 and 5.0 wt.%). Among the synthesized photocatalysts, the 5.0 wt. % AuSe QDs/ $\text{Cs}_2\text{Fe}_2\text{O}_4$  NC sample showed high photoactivity for the RhB degradation may be due to surface plasmon resonance (SPR), synergistic effect and its smallest energy gap. The coexistence of AuSe QDs and  $\text{Cs}_2\text{Fe}_2\text{O}_4$  NC in the prepared photocatalysts confirmed by TEM images and XRD patterns. The photocatalytic activity of the pure  $\text{Cs}_2\text{Fe}_2\text{O}_4$ , 1.0, 2.5, 5.0 wt.% AuSe QDs/ $\text{Cs}_2\text{Fe}_2\text{O}_4$  NC photocatalysts for degradation of RhB dye, was 50.0 %, 59.1 %, 76.4 %, and 99.15 % after 150 min under visible light, respectively, which confirms that the separation of photogenerated holes and electrons have been significantly enhanced, in turn to degradation of RhB dye easily. The results showed that AuSe QDs/ $\text{Cs}_2\text{Fe}_2\text{O}_4$  NCs were stable and efficient photocatalysts, that act as promising photocatalysts for water environmental remediation.

#### Declarations

##### Author contribution statement

Fares T. Alshorifi Conceived and designed the experiments; Performed the experiments; Analyzed and interpreted the data; Wrote the paper.

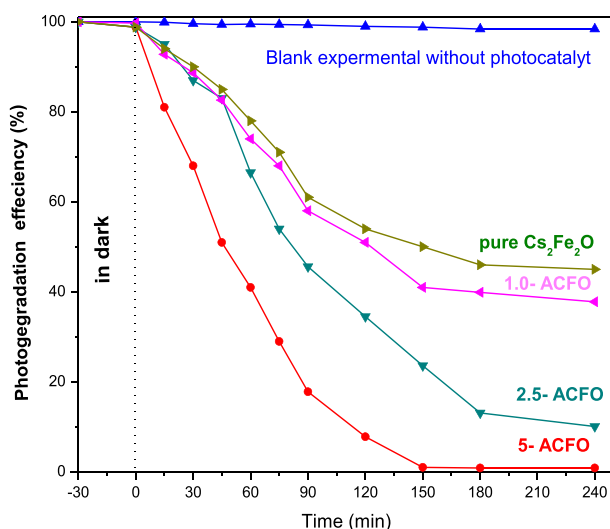


**Figure 7.** Photocatalytic performance of pure  $\text{Cs}_2\text{Fe}_2\text{O}_4$  NC and  $x$  wt.% AuSe QDs/ $\text{Cs}_2\text{Fe}_2\text{O}_4$  NCs.

Abdullah A. Alswat: Contributed reagents, materials, analysis tools or data; Wrote the paper.

Reda S. Salama: Performed the experiments; Analyzed and interpreted the data; Contributed reagents, materials, analysis tools or data; Wrote the paper.

#### Funding statement

This research did not receive any specific grant from funding agencies in the public, commercial, or not-for-profit sectors.

#### Data availability statement

Data will be made available on request.

#### Declaration of interests statement

The authors declare no conflict of interest.

#### Additional information

No additional information is available for this paper.

#### References

- [1] A. Salem, E. Saion, N.M. Al-Hada, H.M. Kamari, A.H. Shaari, S. Radiman, Simple synthesis of ZnSe nanoparticles by thermal treatment and their characterization, *Results Phys.* 7 (2017) 1175–1180.
- [2] M. Heidari, N. Sattarahmady, N. Azarpira, H. Heli, A.R. Mehdizadeh, T. Zare, Photothermal cancer therapy by gold-ferrite nanocomposite and near-infrared laser in animal model, *Laser Med. Sci.* 31 (2016) 221–227.
- [3] R.S. Salama, M.A. Mannaa, H.M. Altass, A.A. Ibrahim, A.E.R.S. Khder, Palladium supported on mixed-metal-organic framework (Co-Mn-MOF-74) for efficient catalytic oxidation of CO, *RSC Adv.* 11 (2021) 4318–4326.
- [4] R.S. Salama, E.S.M. El-Sayed, S.M. El-Bahy, F.S. Awad, Silver nanoparticles supported on UiO-66 (Zr): as an efficient and recyclable heterogeneous catalyst and efficient adsorbent for removal of indigo carmine, *Colloids Surfaces A Physicochem. Eng. Asp.* 626 (2021) 127089.
- [5] H.M. Altass, M. Morad, A.E.-R.S. Khder, M.A. Mannaa, R.S. Jassas, A.A. Alsimeere, S.A. Ahmed, R.S. Salama, Enhanced catalytic activity for CO oxidation by highly active Pd nanoparticles supported on reduced graphene oxide/copper metal organic framework, *J. Taiwan Inst. Chem. Eng.* 128 (2021) 194–208.
- [6] S.K. Srikan, D.D. Giri, D.B. Pal, P.K. Mishra, S.N. Upadhyay, Green synthesis of silver nanoparticles: a review, *Green Sustain. Chem.* 6 (2016) 34–56.
- [7] H.M. Altass, M. Morad, A.S. Khder, M. Raafat, R.I. Alsantali, M.A. Khder, R.S. Salama, M.S. Malik, Z. Moussa, M.A.S. Abourehab, Exploitation the unique acidity of novel cerium-tungstate catalysts in the preparation of indole derivatives under eco-friendly acid catalyzed Fischer indole reaction protocol, *Arab. J. Chem.* 15 (2022) 103670.
- [8] L. Cai, Z. Zhang, H. Xiao, S. Chen, J. Fu, An eco-friendly imprinted polymer based on graphene quantum dots for fluorescent detection of p-nitroaniline, *RSC Adv.* 9 (2019) 41383–41391.
- [9] N. Tang, Y. Li, F. Chen, Z. Han, In situ fabrication of a direct Z-scheme photocatalyst by immobilizing CdS quantum dots in the channels of graphene-hybridized and supported mesoporous titanium nanocrystals for high photocatalytic performance under visible light, *RSC Adv.* 8 (2018) 42233–42245.
- [10] K. Cao, M.-M. Chen, F.-Y. Chang, Y.-Y. Cheng, L.-J. Tian, F. Li, G.-Z. Deng, C. Wu, The biosynthesis of cadmium selenide quantum dots by Rhodotorula mucilaginosa PA-1 for photocatalysis, *Biochem. Eng. J.* 156 (2020) 107497.
- [11] S.A. El-Hakam, F.T. AlShorifi, R.S. Salama, S. Gamal, W.S.A. El-Yazeed, A.A. Ibrahim, A.I. Ahmed, Application of nanostructured mesoporous silica/bismuth vanadate composite catalysts for the degradation of methylene blue and brilliant green, *J. Mater. Res. Technol.* 18 (2022) 1963–1976.
- [12] F.T. Alshorifi, A.A. Alswat, M.A. Mannaa, M.T. Alotaibi, S.M. El-bahy, R.S. Salama, Facile and green synthesis of silver quantum dots immobilized onto a polymeric CTS – PEO blend for the photocatalytic degradation of p - nitrophenol, *ACS Omega* 6 (2021) 30432–30441.
- [13] M.A. Mannaa, K.F. Qasim, F.T. Alshorifi, S.M. El-Bahy, R.S. Salama, Role of NiO nanoparticles in enhancing structure properties of TiO<sub>2</sub> and its applications in photodegradation and hydrogen evolution, *ACS Omega* 6 (2021) 30386–30400.
- [14] R. Wang, X. Wei, J. Xie, B. Wang, X. He, One-step synthesis of CdSe quantum dots by using hydrazine hydrate reduction of selenium dioxide, *Aust. J. Chem.* 71 (2018) 524–526.
- [15] H.K. Han, J.C. Huang, H. Qi, D.Y. Lu, Preparation of ZnSe quantum dots by hydrothermal method assisted by ammonia, in: *Mater. Sci. Forum, Trans Tech Publ.*, 2019, pp. 99–106.
- [16] E. Soheyli, R. Sahraei, G. Nabiyouni, Preparation of highly biocompatible ZnSe quantum dots using a new source of acetyl cysteine as capping agent, *J. Fluoresc.* 27 (2017) 1581–1586.
- [17] P. Shao, H. Wang, Q. Zhang, Y. Li, White light emission from Mn-doped ZnSe d-dots synthesized continuously in microfluidic reactors, *J. Mater. Chem. B* 21 (2011) 17972–17977.
- [18] D.M. Kroupa, D.H. Arias, J.L. Blackburn, G.M. Carroll, D.B. Granger, J.E. Anthony, M.C. Beard, J.C. Johnson, Control of energy flow dynamics between tetracene ligands and PbS quantum dots by size tuning and ligand coverage, *Nano Lett.* 18 (2018) 865–873.
- [19] K.-W. Jung, S. Lee, Y.J. Lee, Synthesis of novel magnesium ferrite (MgFe<sub>2</sub>O<sub>4</sub>)/biochar magnetic composites and its adsorption behavior for phosphate in aqueous solutions, *Bioprocess. Technol.* 245 (2017) 751–759.
- [20] H.M. Altass, A.S. Khder, S.A. Ahmed, M. Morad, A.A. Alsabe, R.S. Jassas, K. Althagafy, A.I. Ahmed, R.S. Salama, Highly efficient, recyclable cerium-phosphate solid acid catalysts for the synthesis of tetrahydrocarbazole derivatives by Borsche-Drechsel cyclization, *React. Kinet. Mech. Catal.* 134 (2021) 143–161.
- [21] F. Zia, N. Ghafoor, M. Iqbal, S. Mehboob, Green synthesis and characterization of silver nanoparticles using Cydonia oblong seed extract, *Appl. Nanosci.* 6 (2016) 1023–1029.
- [22] S. D'Addato, D. Pinotti, M.C. Spadaro, G. Paolicelli, V. Grillo, S. Valeri, L. Pasquali, L. Bergamini, S. Corni, Influence of size, shape and core-shell interface on surface plasmon resonance in Ag and Ag@MgO nanoparticle films deposited on Si/SiO<sub>x</sub>, *Beilstein J. Nanotechnol.* 6 (2015) 404–413.
- [23] M. Ghorbanpour, Amine accessibility and chemical stability of silver SPR chips silanised with APTES via vapour phase deposition method, *J. Phys. Sci.* 27 (2016).
- [24] Y.-W. Ma, Z.-W. Wu, L.-H. Zhang, J. Zhang, G.-S. Jian, S. Pan, Theoretical study of the local surface plasmon resonance properties of silver nanosphere clusters, *Plasmonics* 8 (2013) 1351–1360.
- [25] Y. Peng, B. Xiong, L. Peng, H. Li, Y. He, E.S. Yeung, Recent advances in optical imaging with anisotropic plasmonic nanoparticles, *Anal. Chem.* 87 (2015) 200–215.
- [26] H. Liu, B. Wang, E.S.P. Leong, P. Yang, Y. Zong, G. Si, J. Teng, S.A. Maier, Enhanced surface plasmon resonance on a smooth silver film with a seed growth layer, *ACS Nano* 4 (2010) 3139–3146.
- [27] F. Flory, L. Escoubas, G. Berginc, Optical properties of nanostructured materials: a review, *J. Nanophotonics* 5 (2011) 52502.
- [28] C. Ravikant, P. Arun, Plasmon coupling and aging effect in CsCl-Ag thin films, *Mater. Res. Express* 5 (2018) 96405.
- [29] T. Lu, S. Dong, C. Zhang, L. Zhang, G. Cui, Fabrication of transition metal selenides and their applications in energy storage, *Coord. Chem. Rev.* 332 (2017) 75–99.
- [30] S.J. Ahlers, M.-M. Pohl, J. Radnik, D. Linke, E. V Kondratenko, Catalytic role and location of cs promoter in Cs-Au/TiO<sub>2</sub> catalysts for propanol synthesis from CO<sub>2</sub>, C<sub>2</sub>H<sub>4</sub> and H<sub>2</sub>, *Appl. Catal. B Environ.* 176 (2015) 570–577.
- [31] S. Vorobyev, M. Likhtatski, A. Romanchenko, N. Maksimov, S. Zharkov, A. Krylov, Y. Miklin, Colloidal and deposited products of the interaction of tetrachloroauric acid with hydrogen selenide and hydrogen sulfide in aqueous solutions, *Minerals* 8 (2018) 492.
- [32] L.F.E. Machogo, M. Mthimunye, R.K. Sithole, P. Tetyana, N. Phao, G.N. Ngubeni, M. Mlambo, P.S. Mduli, P.M. Shumbula, N. Moloto, Elucidating the structural properties of gold selenide nanostructures, *New J. Chem.* 43 (2019) 5773–5782.
- [33] N.A.N. Mohamad, N.A. Arham, J. Jai, A. Hadi, Plant extract as reducing agent in synthesis of metallic nanoparticles: a review, in: *Adv. Mater. Res., Trans Tech Publ.*, 2014, pp. 350–355.
- [34] H.S. Dosanjh, Synthesis and characterization of pure Cs ferrite and mixed Cs-Li ferrite and their application in adsorption of dyes, *Eur. J. Mol. Clin. Med.* 7 (2020) 3669–3674.
- [35] N.M. Deraz, Facile and eco-friendly route for green synthesis of magnesium ferrite nano particles, *Sci. Sinter.* 52 (2020) 53–65.
- [36] J.-L. Brisset, B. Benstaali, D. Moussa, J. Fanmoe, E. Njoyim-Tamungang, Acidity control of plasma-chemical oxidation: applications to dye removal, urban waste abatement and microbial inactivation, *Plasma Sources Sci. Technol.* 20 (2011) 34021.
- [37] G. Zhu, H. Fang, Y. Xiao, A.S. Hursthouse, The application of fluorescence spectroscopy for the investigation of dye degradation by chemical oxidation, *J. Fluoresc.* 30 (2020) 1271–1279.
- [38] H. An, Y. Qian, X. Gu, W.Z. Tang, Biological treatment of dye wastewaters using an anaerobic-oxic system, *Chemosphere* 33 (1996) 2533–2542.
- [39] D. Bhatia, N.R. Sharma, J. Singh, R.S. Kanwar, Biological methods for textile dye removal from wastewater: a review, *Crit. Rev. Environ. Sci. Technol.* 47 (2017) 1836–1876.
- [40] Y. Wang, R. Wang, N. Lin, Y. Wang, X. Zhang, Highly efficient microwave-assisted Fenton degradation bisphenol A using iron oxide modified double perovskite intercalated montmorillonite composite nanomaterial as catalyst, *J. Colloid Interface Sci.* 594 (2021) 446–459.
- [41] Y. Wang, L. Yu, R. Wang, Y. Wang, X. Zhang, Reactivity of carbon spheres templated Ce/LaCoO<sub>3</sub>. 5CuO<sub>2</sub>. 5O<sub>3</sub> in the microwave induced H<sub>2</sub>O<sub>2</sub> catalytic degradation of salicylic acid: characterization, kinetic and mechanism studies, *J. Colloid Interface Sci.* 574 (2020) 74–86.
- [42] M.A. Mannaa, H.M. Altass, R.S. Salama, MCM-41 grafted with citric acid: the role of carboxylic groups in enhancing the synthesis of xanthenes and removal of heavy metal ions, *Environ. Nanotechnol. Monit. Manag.* 15 (2021) 100410.
- [43] S.A. El-Hakam, S.E. Samra, S.M. El-Dafrawy, A.A. Ibrahim, R.S. Salama, A.I. Ahmed, Synthesis of sulfamic acid supported on Cr-MIL-101 as a heterogeneous acid catalyst and efficient adsorbent for methyl orange dye, *RSC Adv.* 8 (2018) 20517–20533.

- [44] R.S. Salama, S.M. El-Bahy, M.A. Mannaa, Sulfamic acid supported on mesoporous MCM-41 as a novel, efficient and reusable heterogenous solid acid catalyst for synthesis of xanthene, dihydropyrimidinone and coumarin derivatives, *Colloids Surfaces A Physicochem. Eng. Asp.* 628 (2021) 127261.
- [45] A.A. Ibrahim, R.S. Salama, S.A. El-Hakam, A.S. Khder, A.I. Ahmed, Synthesis of sulfated zirconium supported MCM-41 composite with high-rate adsorption of methylene blue and excellent heterogeneous catalyst, *Colloids Surfaces A Physicochem. Eng. Asp.* 616 (2021) 126361.
- [46] S.A. El-Hakam, A.A. Ibrahim, L.A. Elatwy, W.S.A. El-Yazeed, R.S. Salama, Y.G. Abou El-Reash, A.I. Ahmed, Greener route for the removal of toxic heavy metals and synthesis of 14-aryl-14H dibenzo [a, j] xanthene using a novel and efficient Ag-Mg bimetallic MOF as a recyclable heterogeneous nanocatalyst, *J. Taiwan Inst. Chem. Eng.* 122 (2021) 176–189.
- [47] R.S. Salama, S.A. El-Hakam, S.E. Samraa, S.M. El-Dafrawya, A.I. Ahmeda, Adsorption, equilibrium and kinetic studies on the removal of methyl orange dye from aqueous solution by using of copper metal organic framework (Cu-BDC), *Int. J. Mod. Chem.* 10 (2018) 195–207.
- [48] Y. Yang, W. Ji, X. Li, Z. Zheng, F. Bi, M. Yang, J. Xu, X. Zhang, Insights into the degradation mechanism of perfluoroctanoic acid under visible-light irradiation through fabricating flower-shaped Bi<sub>5</sub>O<sub>7</sub>I/ZnO nm heterojunction microspheres, *Chem. Eng. J.* 420 (2021) 129934.
- [49] Y. Yang, Z. Zheng, M. Yang, J. Chen, C. Li, C. Zhang, X. Zhang, In-situ fabrication of a spherical-shaped Zn-Al hydrotalcite with BioCl and study on its enhanced photocatalytic mechanism for perfluoroctanoic acid removal performed with a response surface methodology, *J. Hazard Mater.* 399 (2020) 123070.
- [50] S. Wen, Y. Hui, W. Chuang, Biosynthesis and antioxidation of nano-selenium using lemon juice as a reducing agent, *Green Process. Synth.* 10 (2021) 178–188.
- [51] C. Deraadt, L. Salmon, S. Gatard, R. Ciganda, R. Hernandez, J. Ruiz, D. Astruc, Sodium borohydride stabilizes very active gold nanoparticle catalysts, *Chem. Commun.* 50 (2014) 14194–14196.
- [52] L.F.E. Machogo, R.K. Sithole, N. Phao, T. Kolokoto, S.S. Gqoba, M. Mlamblo, M.J. Moloto, P.M. Shumbula, P.S. Mduli, N. Moloto, Probing the structure and functionalized surface of colloidal AuSe, *Mater. Sci. Eng. B* 263 (2021) 114878.
- [53] M. Gupta, M. Gupta, B.S. Randhawa, Synthesis of nanosized cesium ferrite by precursor and combustion method: a comparative study, *Int. J. Appl. Ceram. Technol.* 10 (2013) 917–923.
- [54] H.M. Zidan, Electron spin resonance and ultraviolet spectral analysis of UV-irradiated PVA films filled with MnCl<sub>2</sub> and CrF<sub>3</sub>, *J. Appl. Polym. Sci.* 88 (2003) 104–111.
- [55] H.M. Zidan, A. Tawansi, M. Abu-Elnader, Miscibility, optical and dielectric properties of UV-irradiated poly (vinylacetate)/poly (methylmethacrylate) blends, *Phys. B Condens. Matter* 339 (2003) 78–86.
- [56] E.A. El-Sayed, G.B. Sakr, Effect of composition on the optical properties of the quaternary Cu<sub>x</sub>Ag<sub>1-x</sub>Te<sub>2</sub> thin films, *Phys. Status Solidi* 198 (2003) 188–196.
- [57] W.S.A. El-Yazeed, S.A. El-Hakam, R.S. Salama, A.A. Ibrahim, A.I. Ahmed, Ag-PMA supported on MCM-41: surface acidity and catalytic activity, *J. Sol. Gel Sci. Technol.* 102 (2022) 387–399.
- [58] A.M. Bakry, W.M. Alamiyer, R.S. Salama, M.S. El-Shall, F.S. Awad, Remediation of water containing phosphate using ceria nanoparticles decorated partially reduced graphene oxide (CeO<sub>2</sub>-PRGO) composite, *Surface. Interfac.* 31 (2022) 102006.
- [59] H.M. Altass, S.A. Ahmed, R.S. Salama, Z. Moussa, R.S. Jassas, R.I. Alsantali, M.M. Al-Rooqi, A.A. Ibrahim, M.A. Khder, M. Morad, Low temperature CO oxidation over highly active gold nanoparticles supported on reduced graphene oxide@ Mg-BTC nanocomposite, *Catal. Lett.* (2022) 1–11.
- [60] R.S. Salama, Synthesis, characterization and Catalytic activities of sulfuric acid loaded on Copper metal organic frameworks (Cu-BDC), *Delta Univ. Sci. J.* 2 (2019) 2.
- [61] A.A. Ibrahim, R.S. Salama, S.A. El-hakam, A.S. Khder, A.I. Ahmed, Synthesis of 12-tungestophosphoric acid supported on Zr/MCM-41 composite with excellent heterogeneous catalyst and promising adsorbent of methylene blue, *Colloids Surfaces A Physicochem. Eng. Asp.* 631 (2021) 127753.
- [62] R.S. Salama, S.M. Hassan, A.I. Ahmed, W.S.A. El-Yazeed, M.A. Mannaa, The role of PMA in enhancing the surface acidity and catalytic activity of a bimetallic Cr-Mg MOF and its applications for synthesis of coumarin and dihydropyrimidinone derivatives, *RSC Adv.* 10 (2020) 21115–21128.